

## Supporting Information for

# Novel Wide Bandgap Nonfullerene Acceptors for Efficient Tandem Organic Solar Cells

Yuliar Firdaus,<sup>#,\*</sup> Qiao He,<sup>#</sup> Yuanbao Lin, Ferry Anggoro Ardy Nugroho, Vincent M. Le Corre, Emre Yengel, Ahmed H. Balawi, Akmara Seikhan, Frédéric Laquai, Christoph Langhammer, Feng Liu, Martin Heeney<sup>\*</sup> and Thomas D. Anthopoulos<sup>\*</sup>

## 1. Synthetic Procedures

<sup>1</sup>H and <sup>13</sup>C NMR spectra were recorded on a Bruker AV-400 (400 MHz), using the residual solvent resonance of CDCl<sub>3</sub>, and the chemical shifts are given in parts per million. Matrix-assisted laser desorption/ionization time-of-flight (MALDI-TOF) mass spectrometry was performed on a Bruker ultrafleXtreme MALDI-TOF analyzer. Elemental analysis was performed in a Thermo Scientific (Calro Erba) elemental analyzer, configured for the percentage of C, H, and N. UV-vis spectra were recorded on a UV-1601 Shimadzu UV-vis spectrometer. All reactions were carried out in oven-dried glassware under nitrogen using solvents and reagents as commercially supplied, unless otherwise stated.

### *Synthesis of IDTA*

To a solution of C8IDT-CHO (200 mg, 0.28 mmol) and 1,3-diethyl-2-thiobarbituric acid (168 mg, 0.84 mmol) in chloroform (20 mL) was added pyridine (1 mL). The mixture was refluxed overnight and then poured into brine/water (30 mL), extracted with dichloromethane (3 × 30 mL) and organic phase was separated, dried over anhydrous Mg<sub>2</sub>SO<sub>4</sub> and concentrated under vacuum. The crude product was purified by column chromatography over silica (eluent: dichloromethane/petroleum ether = 2/1 (v/v)) giving a purple black solid (282 mg, yield 89%). <sup>1</sup>H NMR (400 MHz, CDCl<sub>3</sub>): δ 8.76 (s, 2H), 7.74 (s, 2H), 7.62 (s, 2H), 4.72-4.57 (m, 8H), 2.11-1.84 (m, 8H), 1.39-1.31 (m, 12H), 1.27-1.01 (m, 48H), 0.83-0.79 (m, 12H). <sup>13</sup>C NMR (100 MHz, CDCl<sub>3</sub>): δ 178.71, 161.44, 161.27, 160.21, 157.29, 156.73, 149.93, 141.43, 139.30, 138.03, 116.35, 109.39, 54.37, 44.14, 43.39, 39.11, 31.92, 30.03, 29.42, 29.34, 24.59, 22.76, 14.25, 12.71, 12.57. MS (MALDI-TOF): m/z 1135.0 (M<sup>+</sup>), Anal. Calc. for C<sub>66</sub>H<sub>94</sub>N<sub>4</sub>O<sub>4</sub>S<sub>4</sub>: C, 67.37; H, 7.59; N, 4.49. Found: C, 67.26; H, 7.68; N, 4.39%.

### *Synthesis of IDTTA*

To a solution of C8IDTT-CHO (200 mg, 0.226 mmol) and 1,3-diethyl-2-thiobarbituric acid (136 mg, 0.68 mmol) in chloroform (20 mL) was added pyridine (1 mL). The mixture was refluxed overnight and then poured into brine/water (30 mL), extracted with dichloromethane (3 × 30 mL) and organic phase was separated, dried over anhydrous Mg<sub>2</sub>SO<sub>4</sub> and concentrated under vacuum. The crude product was purified by column chromatography over silica (eluent: dichloromethane/petroleum ether = 3/1 (v/v)) giving a purple black solid (240 mg, yield 85%). <sup>1</sup>H NMR (400 MHz,

$\text{CDCl}_3$ ):  $\delta$  8.76 (s, 2H), 8.19 (s, 2H), 7.49 (s, 2H), 4.72-4.55 (m, 8H), 2.36-2.00 (m, 8H), 1.49-1.21 (m, 12H), 1.20-0.92 (m, 48H), 0.82-0.61 (m, 12H).  $^{13}\text{C}$  NMR (100 MHz,  $\text{CDCl}_3$ ):  $\delta$  178.73, 161.27, 160.11, 154.92, 153.97, 149.97, 148.23, 147.29, 143.48, 139.54, 138.92, 137.96, 114.92, 109.76, 54.95, 44.20, 43.35, 38.39, 31.92, 31.77, 29.86, 29.36, 29.27, 24.23, 22.74, 14.32, 14.23, 12.74, 12.59. MS (MALDI-TOF): m/z 1247.0 ( $\text{M}^+$ ). Anal. Calc. for C<sub>70</sub>H<sub>94</sub>N<sub>4</sub>O<sub>4</sub>S<sub>6</sub>: C, 69.80; H, 8.34; N, 4.93. Found: C, 69.76; H, 8.44; N, 4.82%.

## 2. Properties of Neat Materials

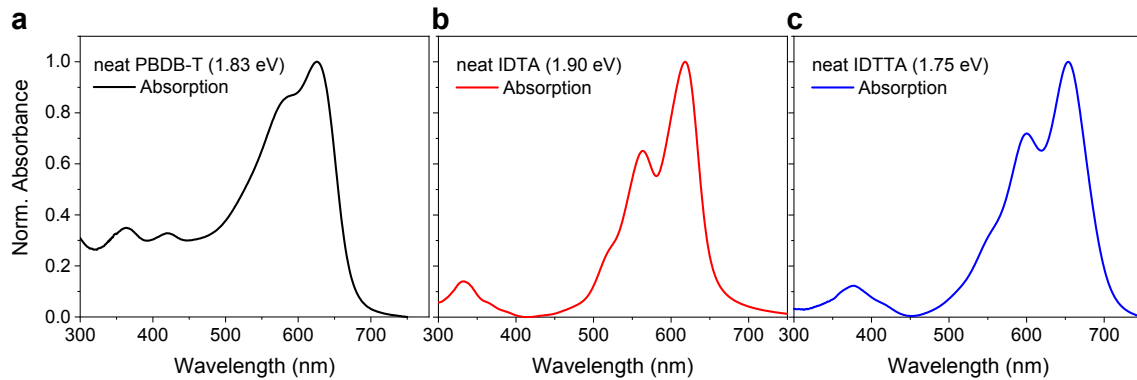


**Fig. S1** The optical band gap of PBDB-T, IDTA, and IDTTA estimated from the onset of absorption spectra of the neat films.

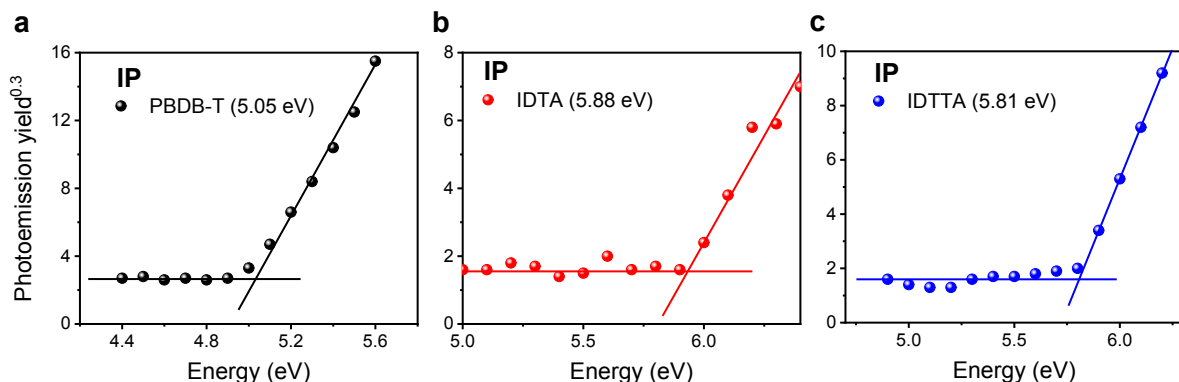


**Fig. S2** PESA curves for neat films of (a) PBDBT, (b) IDTA, and (c) IDTTA. PESA-inferred Ionization potential (IE) values are reported on the plots.

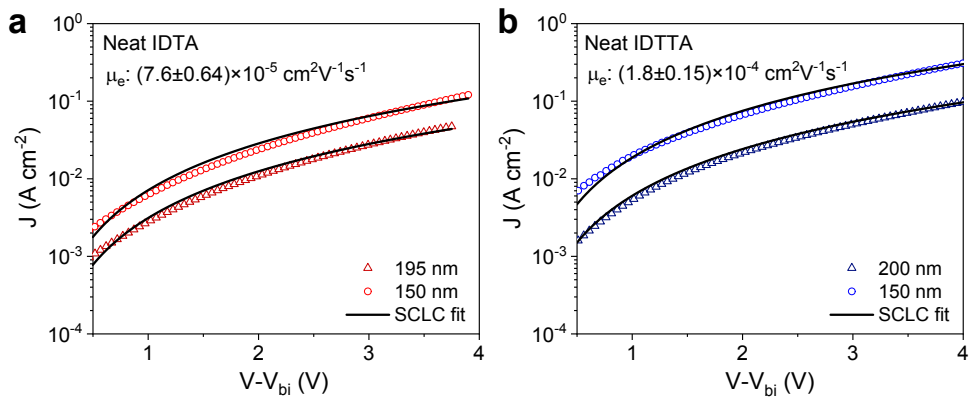


**Fig. S3** Dark current density-voltage (J-V) characteristics for electron-only diodes of (a) neat IDTA, and (b) neat IDTTA films. The electron-only device structure is Glass/ITO/a-ZnO/PFN-Br/neat film/PFN-Br/Al. The solid lines are fits to the experimental data according to the Murgatroyd expression.

### 3. Device Optimizations

**Table S1.** PV performance of the IDTA acceptor in inverted BHJ devices with the polymer donor PBDB-T. Active layers cast from CB, using various donor/acceptor (D/A) ratios. Device area: 0.1 cm<sup>2</sup>.

	ratio	V <sub>OC</sub> (V)	J <sub>SC</sub> (mA cm <sup>-2</sup> )	FF (%)	PCE <sub>max</sub> (%)
PBDB-T:IDTA <sup>a)</sup>	1.5:1	0.99	11.1	58	6.3
	1.25:1	1.00	11.0	58	6.4
	1:1	1.01	10.6	62	6.6
	1:1.25	1.01	11.0	64	7.1
	1:1.5	1.01	10.5	64	6.8
PBDB-T:IDTA <sup>b)</sup>	1.5:1	0.96	11.9	58	6.5
	1.25:1	0.97	11.9	60	6.9
	1:1	0.96	11.7	64	7.2
	1:1.25	0.97	10.6	64	6.6
	1:1.5	0.97	10.8	63	6.6
PBDB-T:IDTA <sup>c)</sup>	1.5:1	0.83	12.0	58	5.8
	1.25:1	0.85	11.7	60	5.9
	1:1	0.86	11.1	62	5.9
	1:1.25	0.85	10.4	61	5.4
	1:1.5	0.82	9.4	54	4.1

<sup>a)</sup> as-cast; <sup>b)</sup> annealing 80°C; <sup>c)</sup> annealing 110 °C.

**Table S2** PV performance of the IDTA acceptor in inverted BHJ devices with the polymer donor PBDB-T; blends cast with various concentration of solution-processing 1,8-Diiodooctane (DIO) and 1-Chloronaphthalene (CN) additives in chlorobenzene (CB).

	Additives (%)	V <sub>OC</sub> (V)	J <sub>SC</sub> (mA cm <sup>-2</sup> )	FF (%)	PCE <sub>max</sub> (%)
PBDB-T:IDTA (DIO) <sup>a)</sup> Ratio 1:1	no	1.00	12.3	60	7.4
	0.25	1.00	11.7	62	7.2
	0.5	1.01	10.1	62	6.3
	1	1.02	7.9	57	4.6
PBDB-T:IDTA (CN) <sup>a)</sup> Ratio 1:1	no	1.00	11.2	59	6.6
	0.25	1.00	11.0	58	6.4
	0.5	1.01	10.9	59	6.5
	1	1.01	10.0	64	6.4

<sup>a)</sup> annealing 80 °C.

**Table S3** PV performance of the IDTTA acceptor in inverted BHJ devices with the polymer donor PBDB-T; Active layers cast for various concentration of solution-processing 1,8-Diiodooctane (DIO) additives in chlorobenzene (CB).

	Condition (Solvent, annealing)	V <sub>OC</sub> (V)	J <sub>SC</sub> (mA cm <sup>-2</sup> )	FF (%)	PCE <sub>max</sub> (%)
PBDB-T:IDTTA ratio 1:1	CB, as-cast	1.02	13.3	67	9.1
	CB, anneal 80°C	1.00	13.3	68	9.1
	CB, anneal 110°C	0.97	13.9	71	9.6
	CB+0.2% DIO, as-cast	1.02	13.3	60	8.2
	CB+0.2% DIO, anneal 110°C	0.96	14.0	69	9.3
	CB+0.5% DIO, as-cast	1.02	13.0	64	8.6
	CB+0.5% DIO, anneal 110°C	1.01	13.0	67	8.7
	CB+1% DIO, as-cast	0.99	12.8	68	8.6
	CB+1% DIO, anneal 110°C	0.96	12.8	58	7.2
	CB+0% CN, anneal 110°C	1.00	13.5	70	9.4
	CB+0.25% CN, anneal 110°C	1.00	13.3	70	9.3
	CB+0.5% CN, anneal 110°C	1.00	13.3	69	9.1
	CB+1% CN, anneal 110°C	1.04	11.7	64	7.7

**Table S4** PV performance of the IDTTA acceptor in inverted BHJ devices with the polymer donor PBDB-T. Active layers cast from chlorobenzene (CB), using various donor/acceptor (D/A) ratios.

	Ratio	V <sub>OC</sub> (V)	J <sub>SC</sub> (mA cm <sup>-2</sup> )	FF (%)	PCE <sub>max</sub> (%)
PBDB-T:IDTTA CB, anneal 110°C	1.5:1	0.95	15.2	58	8.4
	1.25:1	0.94	15.0	61	8.6
	1:1	0.97	14.5	71	9.9
	1:1.25	0.94	14.1	55	7.3
	1:1.5	0.91	13.7	49	6.1

**Table S5** Performance parameters of OPV with wide band gap (both donor and acceptor component) in recent years ( $E_g^{\text{opt}}$  between 1.7 to 2.0 eV).

Acceptor	bandgap (eV)	Donor	Bandgap (eV)	PCE(%)	Reference
IDTTA	1.75	PBDB-T	1.84	10.8	This work
IDTA	1.90	PBDB-T	1.84	7.38	This work
DICTF	1.82	PBDB-T	1.84	5.93	1
IDT-TBA	1.91	PBDB-T	1.84	5.50	2
IDDT-TBA	1.78	PBDB-T	1.84	7.50	2
Tfif-IC	1.74	PBDB-T-2F	1.80	5.90	3
IDTIC	1.70	PDBT-T1	1.85	7.40	4
DBFI-EDOT	1.70	PSEHTT	1.80	8.10	5
DBFI-T	1.73	PSEHTT	1.80	5.04	6
DICTiF	1.75	PBDB-T	1.84	6.97	7
DTINC6	1.70	PBDB-T	1.84	8.72	8
DTINC8	1.73	PBDB-T	1.84	9.03	8
IDT-IC	1.72	PBDB-T	1.84	5.82	9
P2O2	2.24	PDBT-T1	1.85	2.53	10
P2N2	2.23	PDBT-T1	1.85	3.86	10
P4N4	2.28	PDBT-T1	1.85	5.71	10
TPA-PDI	1.84	PDBT-T1	1.85	4.42	11
TPA-PDI-S	1.94	PDBT-T1	1.85	5.66	11
TPA-PDI-Se	1.94	PDBT-T1	1.85	6.10	11
SdiPBI	2.22	PDBT-T1	1.85	8.42	12
TPH	2.19	PDBT-T1	1.85	8.23	13
TPH-Se	2.17	PDBT-T1	1.85	9.28	13
N7	1.82	P3HT	2.00	2.30	14
DPP-FN-DPP	1.75	P3HT	2.00	1.20	15
DPP-ANQ-DPP	1.74	P3HT	2.00	0.70	15
Cz-BAR	2.10	P3HT	2.00	2.00	16
Flu-BAR	2.15	P3HT	2.00	1.28	16
DPP-Tz	1.74	P3HT	2.00	0.43	17
BTA1	2.48	P3HT	2.00	5.24	18
DNIT-TT2T	2.19	P3HT	2.00	1.25	19
SF(DPPFB)4	1.73	P3HT	2.00	4.42	20
SF(DPPB)4	1.76	P3HT	2.00	5.16	20
BT2	1.82	P3HT	2.00	4.93	21
BT2b	1.75	P3HT	2.00	6.08	21
IO-4Cl	1.80	PBDB-T-2F	1.80	9.80	22

#### 4. Recombination and Mobility Studies of BHJ Devices

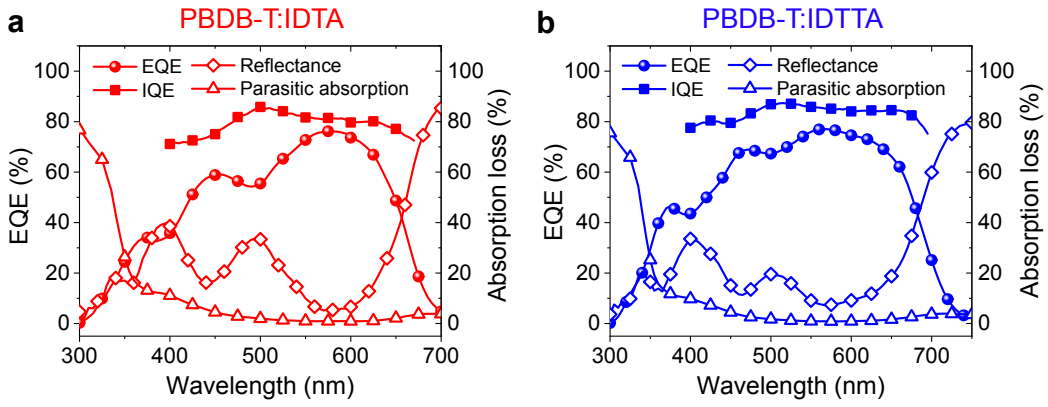


**Fig. S4** EQE, IQE, reflectance (R) and parasitic absorption of optimized BHJ devices of (a) PBDB-T: IDTA and (b) PBDB-T: IDTTA devices.

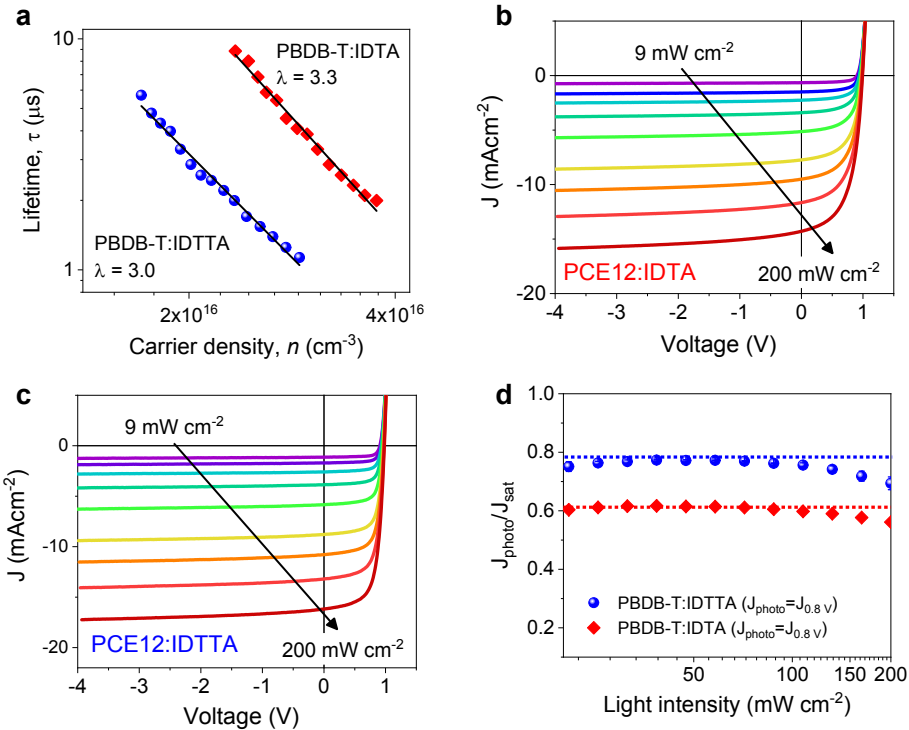


**Fig. S5** (a) Charge carrier lifetime  $\tau$  vs. charge density; carrier lifetime and carrier densities determined from transient-photovoltage (TPV) and charge-extraction (CE) measurements, respectively.  $J$ - $V$  curves vs. light intensity for the optimized BHJ devices of (b) PBDB-T:IDTA device, and (c) PBDB-T:IDTTA. (d)  $J_{\text{photo}}/J_{\text{sat}}$  vs. light intensity at the applied voltage close to  $V_{\text{oc}}$  ( $V=0.8 \text{ V}$ ).

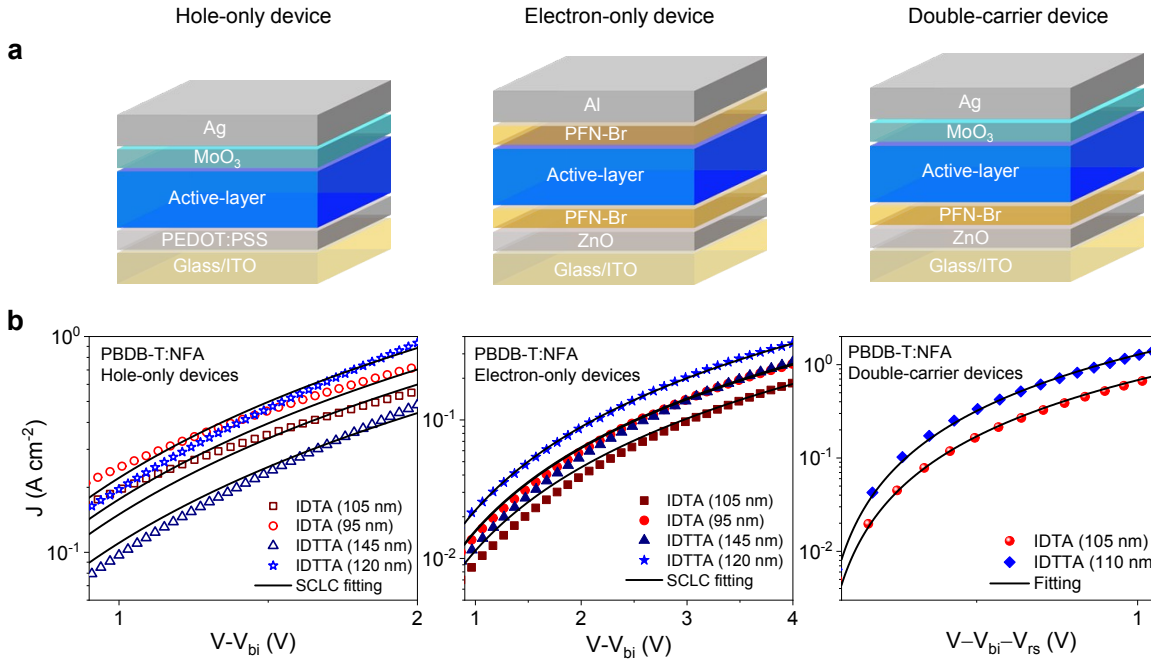


**Fig. S6** (a) Hole-only, electron-only, and double carrier device structures. (b) J-V characteristics measured under dark-condition for hole-only, electron-only, and double carrier devices of PBDB-T:IDTA and PBDB-T:IDTTA blend films (device structures are shown in **Fig. S6a**).

**Table S6.** Average hole ( $\mu_h$ ), electron ( $\mu_e$ ), and effective mobility ( $\mu_D$ ) and recombination characteristics (Langevin recombination rate constant ( $k_L$ ), reduction prefactor ( $\gamma_{pre}$ ), and bimolecular recombination ( $k_{rec}$ )) of PBDB-T:IDTA and PBDB-T:IDTTA OPV devices.

NFA	$\mu_h$ $10^{-4} \text{ cm}^2 \text{ V}^{-1} \text{ s}^{-1}$	$\mu_e$ $10^{-4} \text{ cm}^2 \text{ V}^{-1} \text{ s}^{-1}$	$k_L$ $10^{-10} \text{ cm}^3 \text{ s}^{-1}$	$\mu_D$ $10^{-3} \text{ cm}^2 \text{ V}^{-1} \text{ s}^{-1}$	$\gamma_{pre}$	$k_{rec}$ $\text{cm}^3 \text{ s}^{-1}$
IDTA	$4.4 \pm 0.33$	$0.43 \pm 0.094$	$2.6 \pm 0.19$	$2.3 \pm 0.11$	0.020	$5.4 \times 10^{-12}$
IDTTA	$9.1 \pm 0.48$	$1.0 \pm 0.45$	$5.5 \pm 0.36$	$5.8 \pm 0.55$	0.016	$8.6 \times 10^{-12}$

The prefactor  $\gamma_{pre}$  was determined from the steady-state characterization of single- and double-carrier devices (see **Fig. S6**), using the relation:<sup>23</sup>

$$\gamma_{pre} = \frac{16\pi}{9} \frac{\mu_e \mu_h}{\mu_D^2 - (\mu_e + \mu_h)^2} \quad (\text{S1})$$

**Table S6** Input parameters (charge carrier mobility, recombination rate constant, thickness, HOMO/LUMO level, and IQE) used for the  $J$ - $V$  curve simulation of PBDB-T:IDTA and PBDB-T:IDTTA shown in **Fig. 2a**.

Simulation Input	PBDB-T:IDTA	PBDB-T:IDTTA
IQE (%)	81	88
HOMO/LUMO (eV)	5.2/3.58	5.2/3.59
$\mu_h/\mu_e (10^{-4} \text{ cm}^2 \text{ V}^{-1} \text{ s}^{-1})$	4/0.4	9.1/1
Thickness (nm)	105	105
Prefactor, $\gamma_{\text{pre}}$	0.016	0.023
$k_{\text{BMR}} (10^{-12} \text{ cm}^3 \text{ s}^{-1})$	5.4	8.6

**Table S7** Simulated figure-of-merits ( $V_{\text{OC}}$ ,  $J_{\text{SC}}$ , FF, and PCE) of PBDB-T:IDTA and PBDB-T:IDTTA devices.

Simulation Output	PBDB-T:IDTA	PBDB-T:IDTTA
$V_{\text{OC}}$ (V)	0.986	0.989
$J_{\text{SC}}$ ( $\text{mA cm}^{-2}$ )	11.5	14.4
FF (%)	63	71
PCE (%)	7.16	10.2

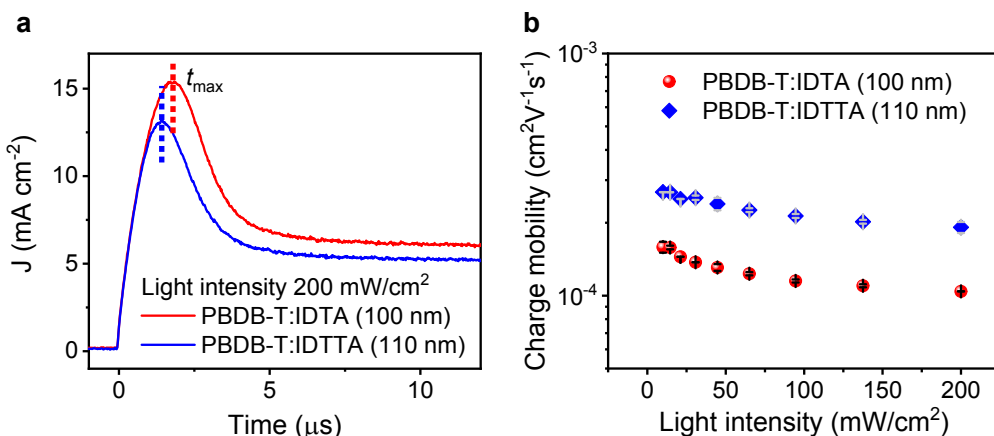


**Fig. S7** (a) Photo-CELIV of the PBDB-T:IDTA and the PBDB-T:IDTTA solar cells at 200  $\text{mW cm}^{-2}$ . (b) Charge carrier mobilities of the PBDB-T:IDTA and the PBDB-T:IDTTA solar cells extracted from the photo-CELIV measurements at different light intensities.

## 5. Additional Morphology Data

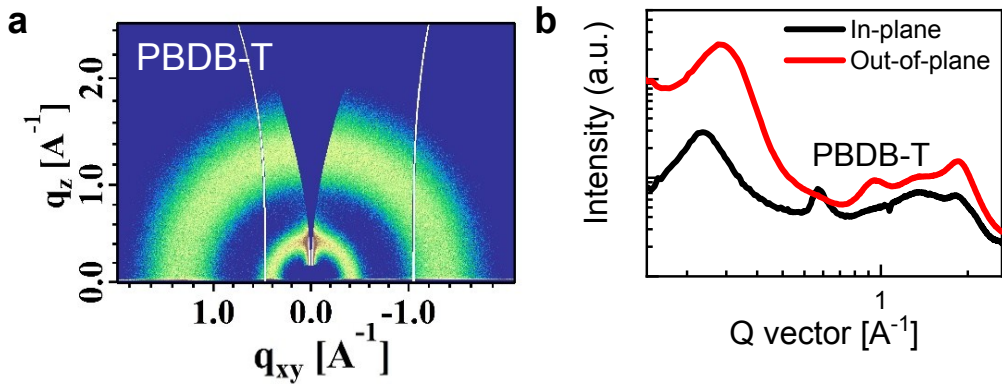


**Fig. S8** (a) 2-D GIWAXS images of neat PBDB-T film. (b) In-plane and out-of-plane line cut profiles of the GIWAXS of the neat PBDB-T film.

## 6. Additional Plasmonic Nanospectroscopy Data

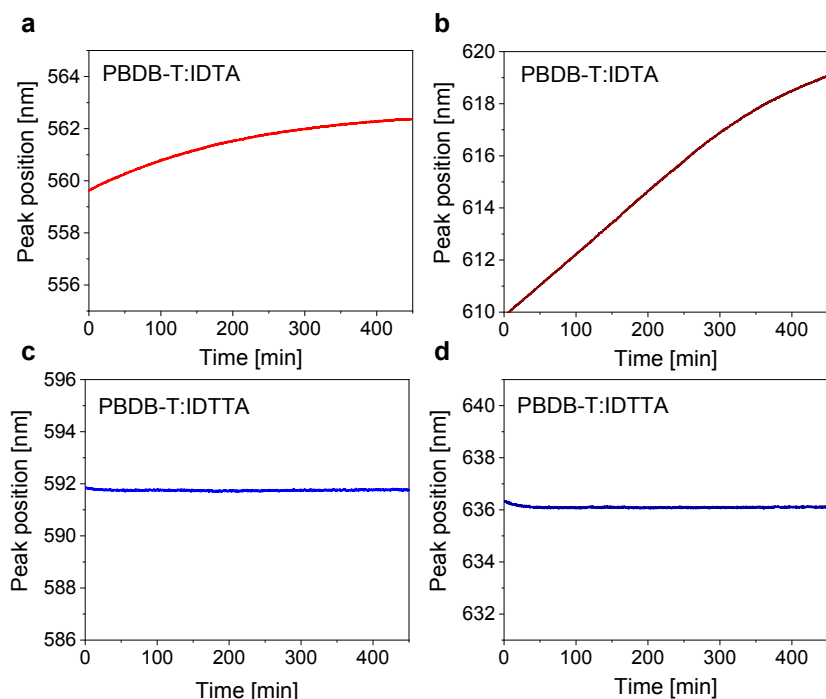


**Fig. S9** The shift of absorption spectra during annealing at 80°C in Argon. (a) peak 1 of PBDB-T:IDTA film, (b) peak 2 of PBDB-T:IDTA film, (c) peak 1 of PBDB-T:IDTTA film, and (d) peak 2 of PBDB-T:IDTTA film.

## 7. Additional Tandem Device Data

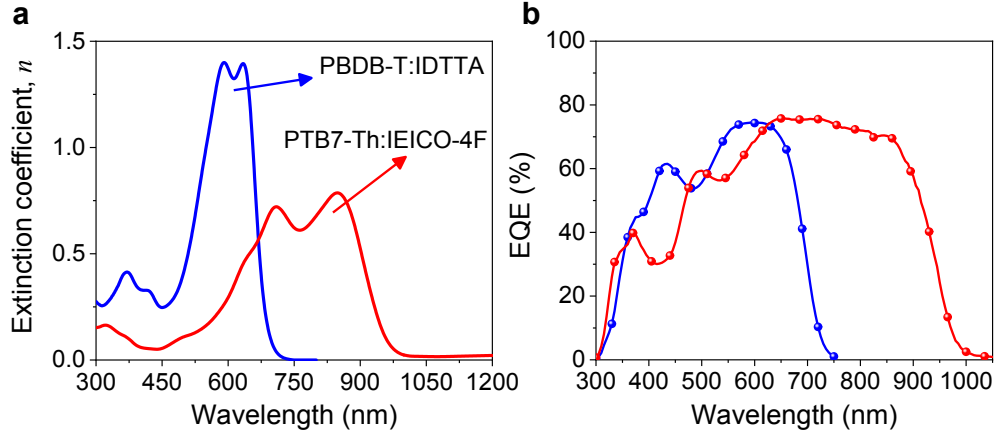


**Fig. S10** (a) Extinction coefficient of PBDB-T:IDTTA and PTB7-Th:IEICO-4F blend films obtained from ellipsometry measurements. (b) EQE spectra of the PBDB-T:IDTTA and PTB7-Th:IEICO-4F single junction devices.

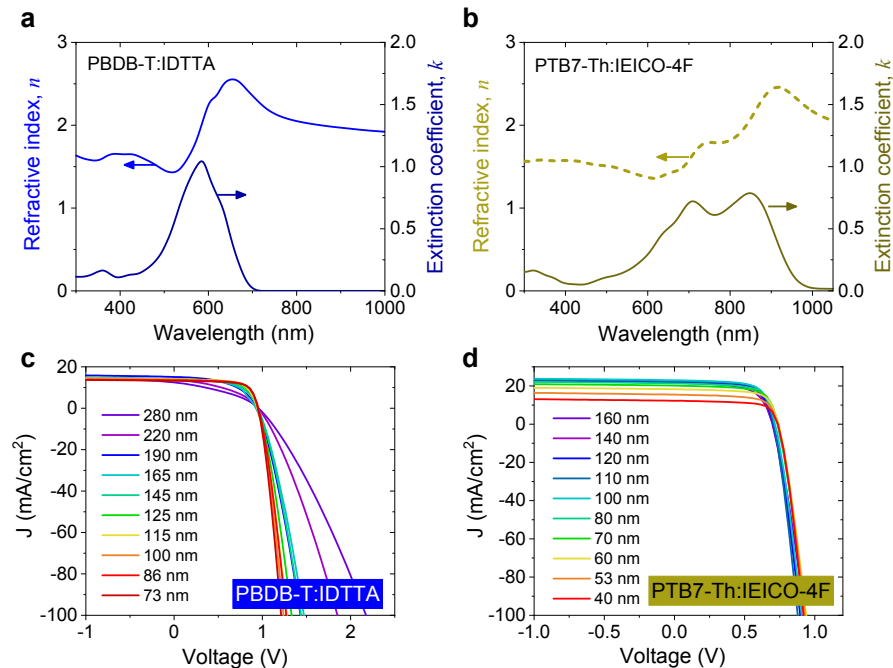


**Fig. S11** Optical constant profiles (extinction coefficient, and refractive index) of (a) PBDB-T:IDTTA, and (b) PTB7-Th:IEICO-4F films obtained from ellipsometry measurements and used for the tandem device modeling. Measured J-V characteristics of (c) PBDB-T:IDTTA, and (d) PTB7-Th:IEICO-4F of different active-layer thicknesses used for the tandem device modeling.

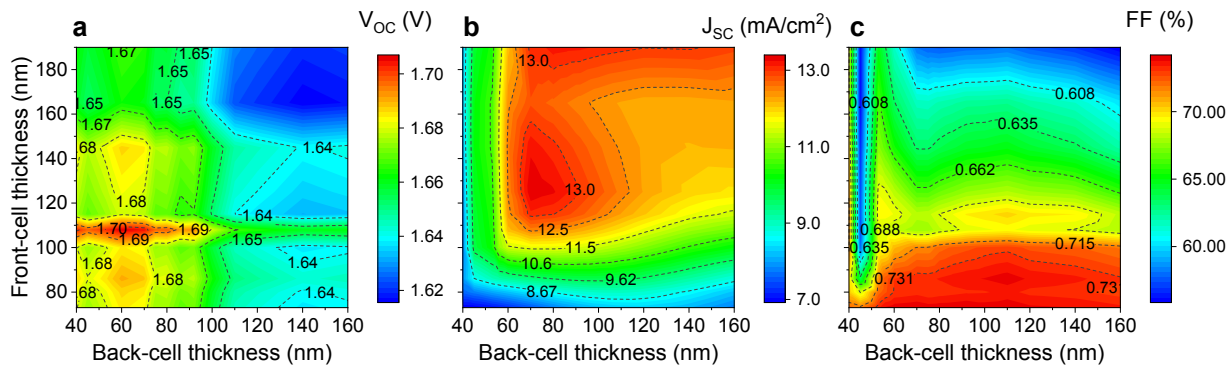


**Fig. S12.** (a)  $V_{OC}$ , (b)  $J_{SC}$ , and (c) FF of tandem OPV devices predicted from optical and electrical modelling.

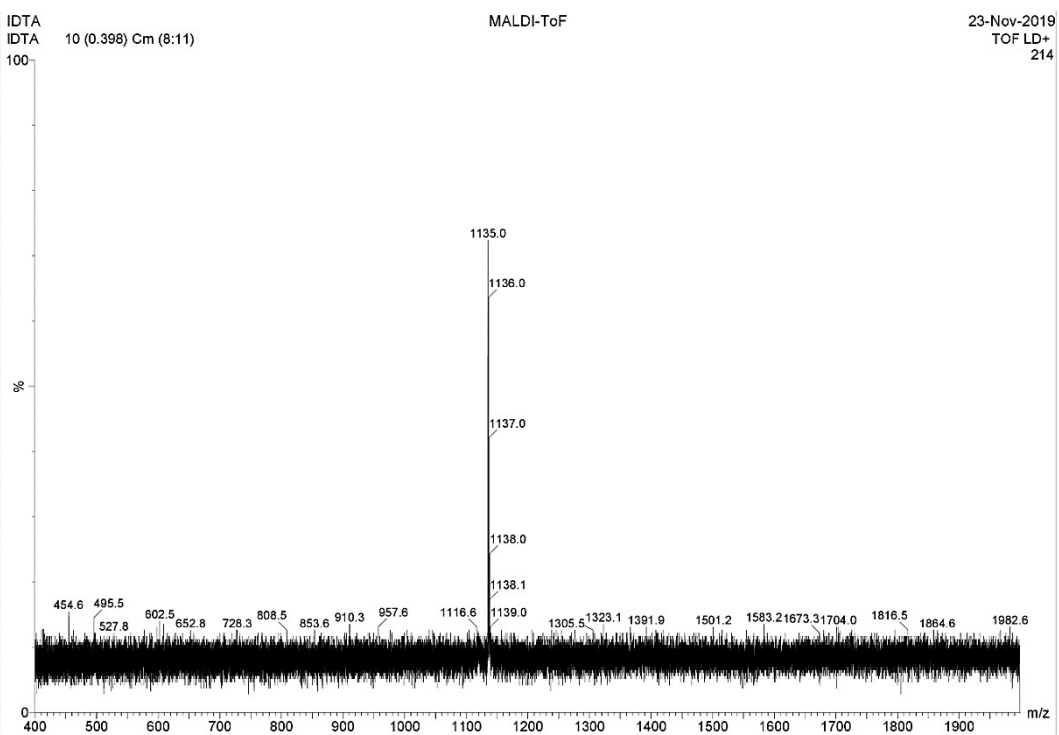


**Fig. S13.** MALDI-TOF MS plot of IDTA.

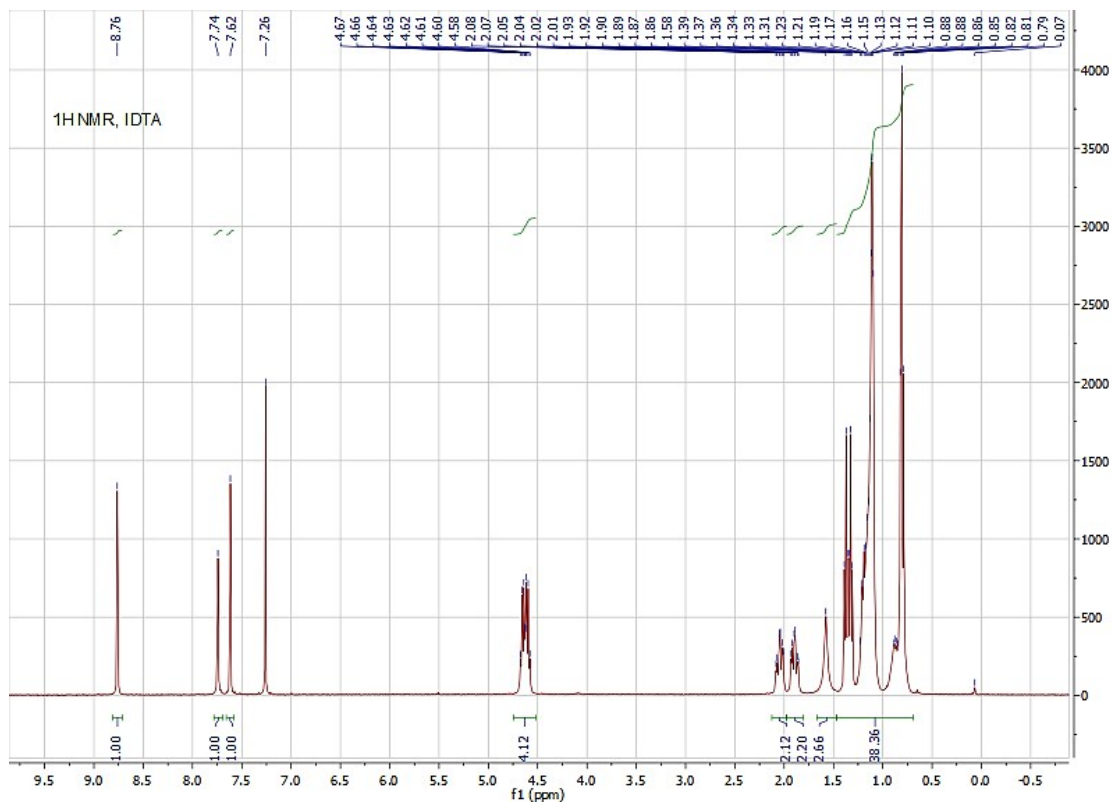


**Fig. S14.** <sup>1</sup>H NMR spectra of IDTA in CDCl<sub>3</sub>.

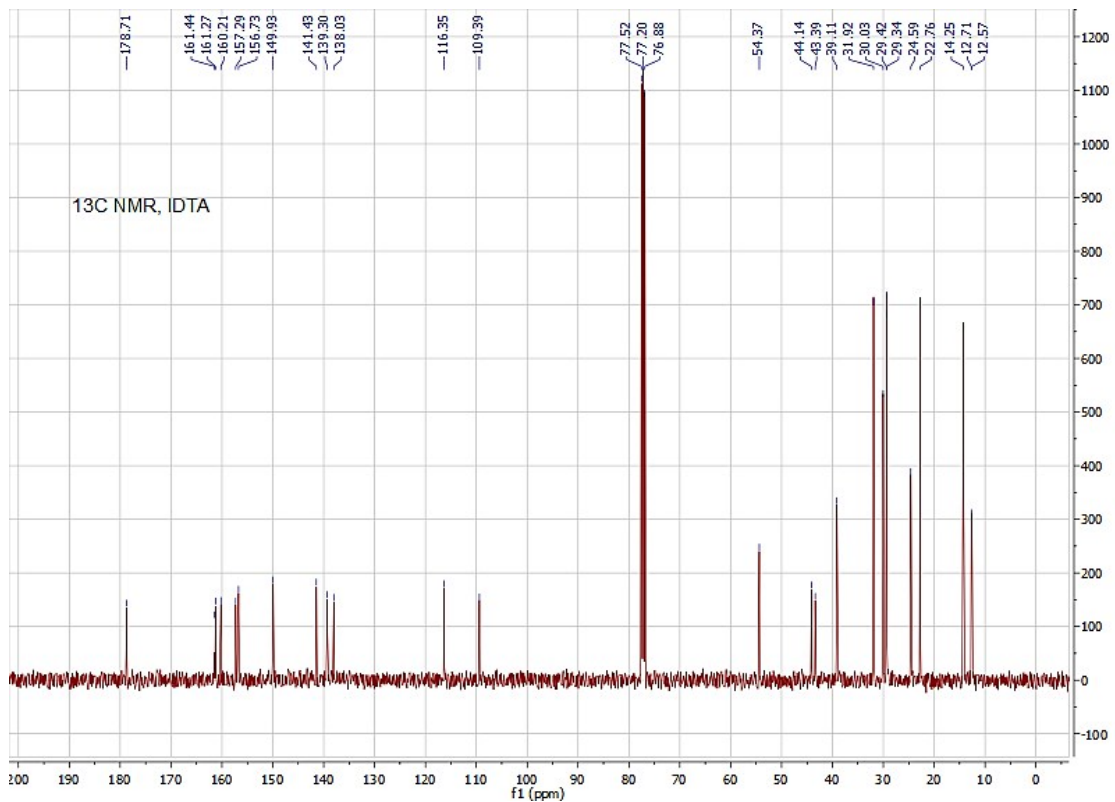


**Fig. S15.** <sup>13</sup>C NMR spectra of IDTA in CDCl<sub>3</sub>.

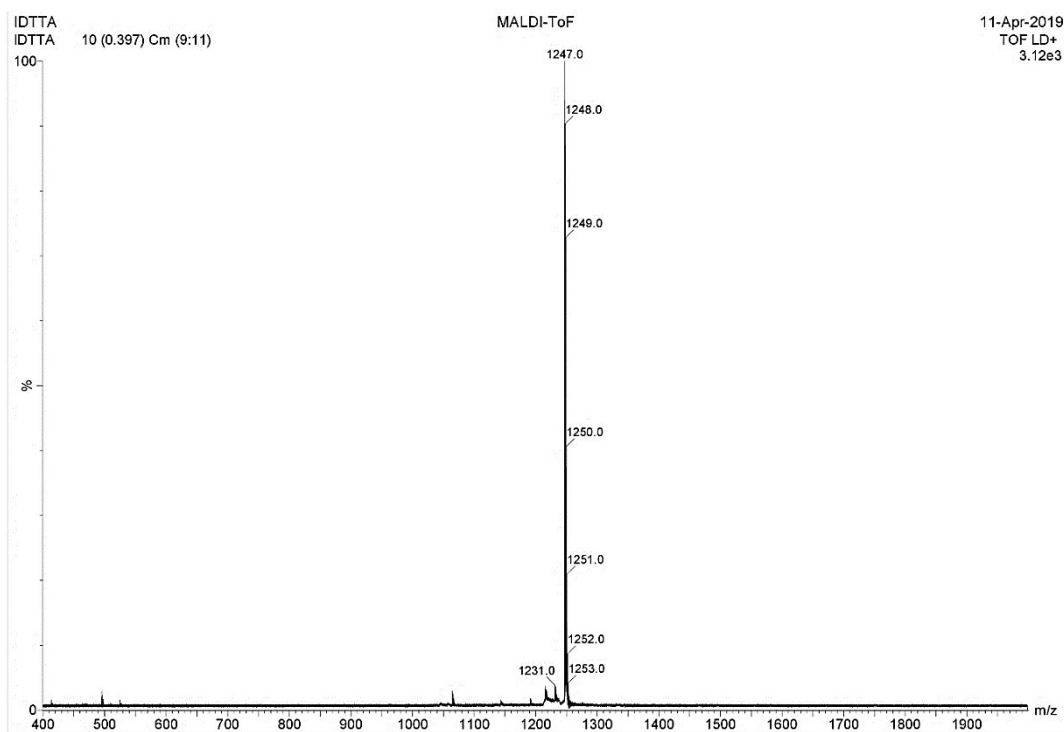


**Fig. S16.** MALDI-TOF MS plot of IDTTA.

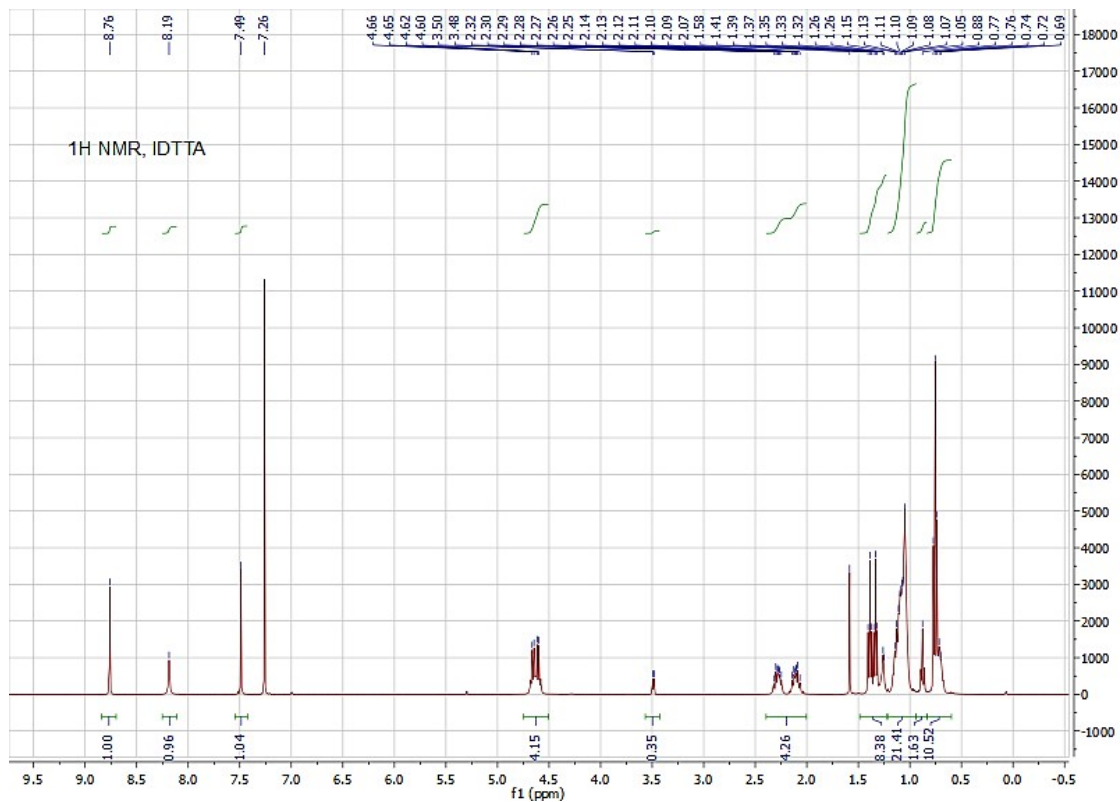


**Fig. S17.** <sup>1</sup>H NMR spectra of IDTTA in CDCl<sub>3</sub>.

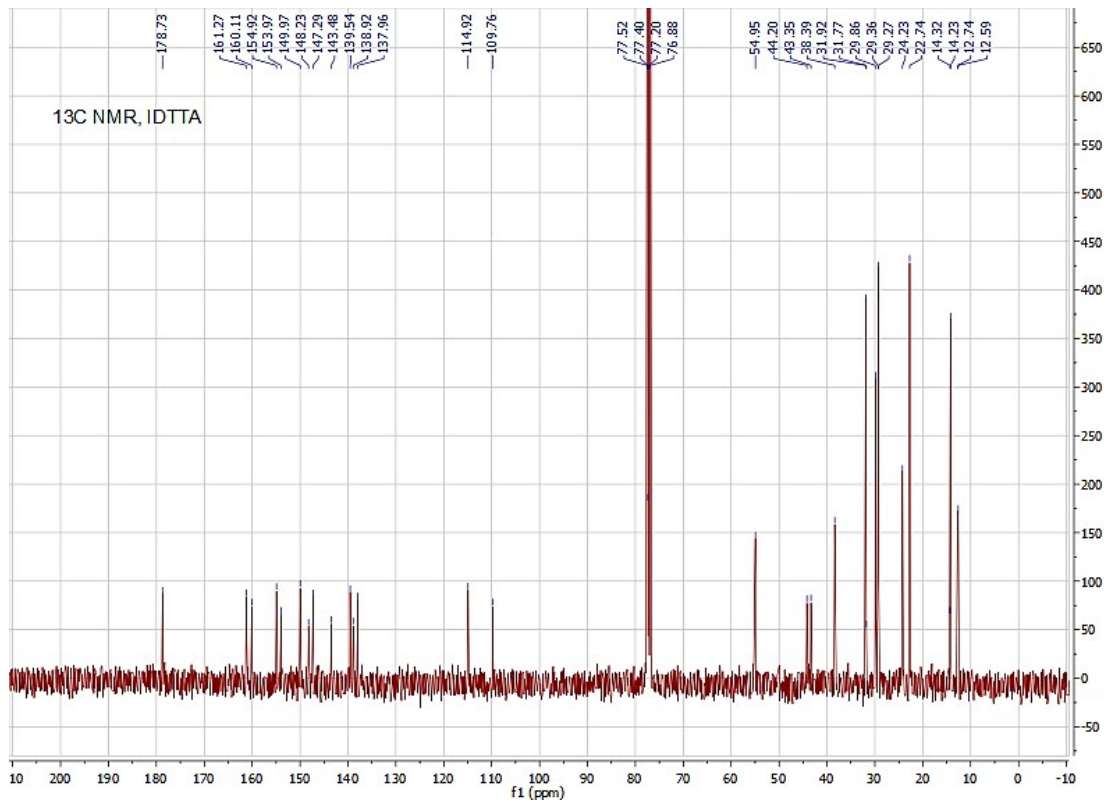


**Fig. S18.** <sup>13</sup>C NMR spectra of IDTTA in CDCl<sub>3</sub>.

## Supporting Information References

- 1 N. Qiu, H. Zhang, X. Wan, C. Li, X. Ke, H. Feng, B. Kan, H. Zhang, Q. Zhang, Y. Lu, Y. Chen, *Adv. Mater.*, 2017, **29**, 1604964.
- 2 Y. Gong, Z. Kan, W. Xu, Y. Wang, S. H. AlShammari, F. Laquai, W.-Y. Lai, W. Huang, *Solar RRL*, 2018, **2**, 1800120.
- 3 G. Liu, J. Jia, K. Zhang, X. e. Jia, Q. Yin, W. Zhong, L. Li, F. Huang, Y. Cao, *Adv. Energy Mater.*, 2019, **9**, 1803657.
- 4 Y. Lin, T. Li, F. Zhao, L. Han, Z. Wang, Y. Wu, Q. He, J. Wang, L. Huo, Y. Sun, C. Wang, W. Ma, X. Zhan, *Adv. Energy Mater.*, 2016, **6**, 1600854.
- 5 Y.-J. Hwang, H. Li, B. A. E. Courtright, S. Subramaniyan, S. A. Jenekhe, *Adv. Mater.*, 2016, **28**, 124.
- 6 H. Li, T. Earmme, G. Ren, A. Saeki, S. Yoshikawa, N. M. Murari, S. Subramaniyan, M. J. Crane, S. Seki, S. A. Jenekhe, *J. Am. Chem. Soc.*, 2014, **136**, 14589.
- 7 H. Zhang, Y. Liu, Y. Sun, M. Li, W. Ni, Q. Zhang, X. Wan, Y. Chen, *Science China Chemistry*, 2017, **60**, 366.
- 8 Y. Ma, M. Zhang, Y. Yan, J. Xin, T. Wang, W. Ma, C. Tang, Q. Zheng, *Chem. Mater.*, 2017, **29**, 7942.
- 9 S. Feng, D. Ma, L. Wu, Y. Liu, C. e. Zhang, X. Xu, X. Chen, S. Yan, Z. Bo, *Science China Chemistry*, 2018, **61**, 1320.
- 10 X. Liu, T. Liu, C. Duan, J. Wang, S. Pang, W. Xiong, Y. Sun, F. Huang, Y. Cao, *J. Mater. Chem.*, 2017, **5**, 1713.
- 11 Z. Luo, W. Xiong, T. Liu, W. Cheng, K. Wu, Y. Sun, C. Yang, *Org. Electron.*, 2017, **41**, 166.
- 12 D. Meng, D. Sun, C. Zhong, T. Liu, B. Fan, L. Huo, Y. Li, W. Jiang, H. Choi, T. Kim, J. Y. Kim, Y. Sun, Z. Wang, A. J. Heeger, *J. Am. Chem. Soc.*, 2016, **138**, 375.
- 13 D. Meng, H. Fu, C. Xiao, X. Meng, T. Winands, W. Ma, W. Wei, B. Fan, L. Huo, N. L. Doltsinis, Y. Li, Y. Sun, Z. Wang, *J. Am. Chem. Soc.*, 2016, **138**, 10184.
- 14 A. M. Raynor, A. Gupta, H. Patil, D. Ma, A. Bilic, T. J. Rook, S. V. Bhosale, *RSC Adv.*, 2016, **6**, 28103.
- 15 T. T. Do, K. Rundel, Q. Gu, E. Gann, S. Manzhos, K. Feron, J. Bell, C. R. McNeill, P. Sonar, *New J. Chem.*, 2017, **41**, 2899.
- 16 E. Lim, *Bull. Korean Chem. Soc.*, 2017, **38**, 285.
- 17 P. Josse, P. Chávez, C. Dindault, C. Dalinot, S. M. McAfee, S. Dabos-Seignon, D. Tondelier, G. Welch, P. Blanchard, N. Leclerc, C. Cabanetos, *Dyes Pigm.*, 2017, **137**, 576.
- 18 B. Xiao, A. Tang, J. Zhang, A. Mahmood, Z. Wei, E. Zhou, *Adv. Energy Mater.*, 2017, **7**, 1602269.
- 19 M. Zhu, J. Miao, Z. Hu, Y. Chen, M. Liu, I. Murtaza, H. Meng, *Dyes Pigm.*, 2017, **142**, 39.
- 20 C. Yuan, W. Liu, M. Shi, S. Li, Y. Wang, H. Chen, C.-Z. Li, H. Chen, *Dyes Pigm.*, 2017, **143**, 217.
- 21 B. Xiao, A. Tang, L. Cheng, J. Zhang, Z. Wei, Q. Zeng, E. Zhou, *Solar RRL*, 2017, **1**, 1700166.
- 22 Y. Cui, Y. Wang, J. Bergqvist, H. Yao, Y. Xu, B. Gao, C. Yang, S. Zhang, O. Inganäs, F. Gao, J. Hou, *Nat. Energy*, 2019, **4**, 768.
- 23 G.-J. A. H. Wetzelaeer, N. J. Van der Kaap, L. J. A. Koster, P. W. M. Blom, *Adv. Energy Mater.*, 2013, **3**, 1130.